Ultra-low Power 2.4GHz RF Energy Harvesting and Storage System with -25dBm Sensitivity

Kenneth Gudan, Shuai Shao, Jonathan J. Hull
Ricoh Innovations Corp.
Menlo Park, CA, USA
gudan@ric.ricoh.com

Joshua Ensworth, Matthew S. Reynolds
University of Washington, Seattle, WA, USA

Abstract— An RF energy harvesting and storage system is described that trickle charges a battery from incident power levels as low as -25 dBm referred to the feedpoint of an 8 dBi patch antenna. The circuit is optimized for the indoor ambient power range typically observed in the 2.4 GHz ISM band so that we can harvest the energy provided by nearby Wi-Fi, Bluetooth and other devices. In this incident power regime, rectified voltages are low, so power management circuit operation in the 100mV regime is critical. We present several improvements to our prior work that significantly improve its performance, including a novel wideband multi-element antenna array, an improved boost converter, and a redesigned battery charger. At -25dBm RF input power, the new harvesting system sources 150μJ into a rechargeable battery after 1 hour. We believe that this work represents the lowest reported startup power yet achieved in battery-storage RF energy harvesting systems.

Keywords—RF Energy Harvesting, Low-Power, Boost Converter, Low-Power Battery Charger

I. INTRODUCTION

Widely deployable, low power wireless sensors enable new applications for the Internet of Things. For example, recent work in sub-threshold circuit design has yielded wireless sensors that calculate and transmit temperature readings every six minutes and consume only 2 μJ [1]. In one proof-of-concept implementation temperature sensors helped reduce the energy costs for a heating, ventilation and air conditioning system by 24% and significantly improved worker efficiency and comfort [2]. Low power image sensors have been reported that can detect motion with a continuous power of 304 nW [3]. In general, it's projected that trillions of new sensors will be needed for IOT applications [4].

Powering large numbers of wireless sensors over a lifetime of years to decades is only practical with energy harvesting. Non-rechargeable batteries of any size have a finite lifetime and the labor cost of replacing them could easily exceed the cost of the sensors. Energy harvesting, on the other hand, has the potential to provide an energy supply over very long time periods. The primary challenge for energy harvesting systems is harvesting power from sources that do not affect the user's environment and that are always available. For example, ambient light is an obvious energy source but it can be easily obscured or unavailable when the room lights are turned off.

RF energy is often provided by ambient sources and could be supplied by active emitters. Recent work showed that in a typical office environment, ambient levels of power down to -20 dBm (at the cable feedpoint of an 8 dBi patch antenna) are abundant in the 2.4 GHz ISM band in which Wi-Fi and Bluetooth devices operate [5]. Previous work in the literature has focused on rectifying this incident RF power into DC and storing it in a capacitor [6-9].

We have previously demonstrated a system architecture that takes into account the bursty nature of the low energy pulses that are typically observed in Wi-Fi traffic as well as the power- and voltage-limited nature of the rectified energy [10]. That paper presented a unique harvester design that charged a NiMH battery over long periods of time. A battery was used because its long-term leakage is much lower than that of a supercapacitor.

This paper presents several significant improvements to the earlier design including a newly developed, wideband antenna array, rectifier, boost converter, and a modified charger circuit. Collectively, these approaches improve the harvester's sensitivity from -20 dBm to -25 dBm while at the same time increasing the amount of energy harvested over a one-minute period by 20X from 100 nJ to 2 μJ, thereby improving the viability of RF harvesting as a power source for wireless sensors. Long harvesting intervals (over a period of minutes to hours or more) are possible with our architecture because we accumulate charge in a battery whereas previous techniques might dissipate that energy in quiescent current in the power harvesting circuit and/or capacitor leakage before enough energy is available to perform a useful task.

Our improved design addresses three technical challenges of RF energy harvesting at ultra-low power levels: (1) antenna design, (2) boost converter optimization, and (3) transferring low voltages into a rechargeable battery. The effect that these changes have on long term performance is illustrated by the results in this paper that show we source 150 μJ into a rechargeable battery after one hour with only -25 dBm input power. This is a significant improvement on our previous work that transferred 5.8 μJ from -20 dBm incident RF power in the same amount of time [10]. Our current results compare very favorably to those considered in a recent RF energy harvesting survey [11]. We believe that this work represents the lowest reported startup power (-25 dBm) yet achieved in battery-storage RF energy harvesting systems.

II. RF Energy Harvesting System Overview

The proposed RF energy harvesting system may be thought of in terms of four key blocks, as shown in Fig. 1. A critical feature of the third component, the boost converter, is startup at ultra-low input voltages, while maintaining high efficiency at useful output voltages. Boost factors of up to 20X may be needed to convert rectified voltages as low as 40mV to a useful voltage of e.g. 800mV to run CMOS logic. Finally, an energy reservoir such as a battery, large capacitor, or supercapacitor is needed to accumulate energy from the incoming RF sources until sufficient energy is available for a sensing operation.

A. Antenna Design

The antenna is one of the most important components of an RF energy harvesting system. It collects ambient RF power and transmits it to the rectifier; therefore it must be designed to capture as much energy as possible. Here our motivation is to design a high gain, low profile, and broadband antenna for power harvesting. Even though the designed system operates in the 2.4GHz ISM band, a broad impedance bandwidth will make the antenna more robust and less susceptible to fabrication errors and environmental changes. We chose a patch antenna for this design because it has a planar structure that is easily manufactured and installed.

In order to make the antenna broadband and compact, a miniaturized antenna element was first designed. Shown in Fig. 2, the antenna element consists of a U-slot structure which enables a broad impedance bandwidth. The antenna is printed on a low loss RO3010 substrate material with a thickness of 6mm and a dielectric constant of 10.2. The radiating element has dimensions of L = 0.155λ = 19mm x W = 0.118λ = 14.5mm. L_s = 10.15mm, L_t = 1mm, W_g = 1mm, x_0 = L/2, y_0 = W/2. The size of the ground plane is 0.326 λ x 0.326 λ (40mm x 40mm).

Antenna arrays are used to increase gain. In ambient harvesting applications, it is important to note that, as opposed to antenna arrays used in communication or radar systems, suppressing the side lobes of the array may not be a priority. The goal is instead to capture as much of the available ambient energy as possible, regardless of the direction of incidence of that energy.

It is well known that increasing the number of elements in an antenna array can increase its gain. However, in the applications we consider such as ambient environmental monitoring, there is a practical size constraint of about 120mm x 120 mm that's based on the space that's deemed acceptable to end users. Furthermore, antennas need to tradeoff directivity and coverage. Antenna arrays with high gain inevitably have narrow coverage which makes them more sensitive to misalignment [12, 13]. Given this tradeoff analysis, we determined that a 2x2 antenna array comprised of the already-designed antenna elements would significantly increase gain with an acceptable decrease in coverage and maintain a low profile. Simulation results show that the proposed antenna array achieves a peak realized gain of 11.5dBi and a 3dB beamwidth of 41 degrees in the E plane, 42 degrees in the H plane.

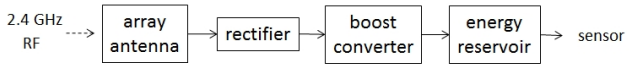

Fig. 1. Block diagram of the RF energy harvesting system.

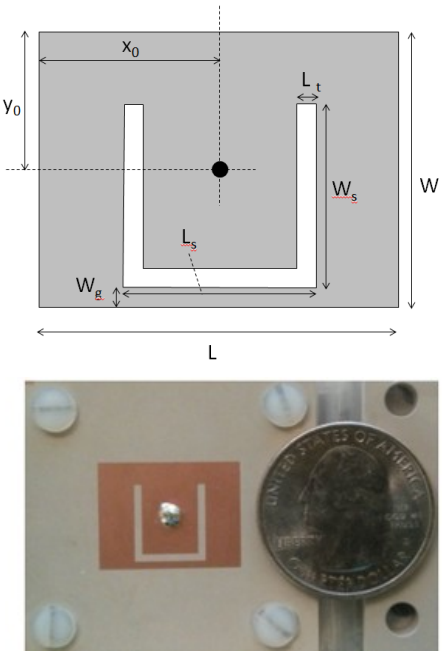

Fig. 2. Individual antenna element.

Shown in Fig. 3, the proposed 2x2 antenna array consists of four identical antenna elements mounted on a backplane of Rogers RO473 substrate with a dielectric constant of 3 and a thickness of 0.76mm. Microstrip transmission lines are printed on one side of the backplane, ground plane is printed on the other side. It is noted that an H shaped ground plane is used in this design instead of a rectangular ground. Such that the individual antenna element preserves the wide bandwidth, therefore the antenna array also achieves a broad impedance bandwidth. The backplane measures 120mm x 120mm, while the element spacing is 80mm. This spacing was driven by the desire to reduce inter-element coupling and maximize gain. Power is combined in RF, rather than DC, to maximize the RF voltage available to the rectifier and thus its efficiency at low input power.

The ground plane of each individual element forms a pressure contact with the H-shaped microstrip ground on the backplane. The feeding network is designed as a microstrip transmission line with parallel feeding. The individual element feeding networks are connected via a through-hole soldering pin. At the center of the array, an SMA connector is soldered to the ground plane and the conductive pin is fed through to the backside and soldered to the feeding network. There is a hole in the array so that the front-mounted SMA cable can be guided through the array and connected to the rest of the harvester without interfering with the individual antenna elements.

B. Rectifier Design

The rectifer is a single stage voltage doubler that uses the Avago HSMS-286C RF detector diodes with microstrip matching networks on Rogers 4003 substrate. We chose this design because our previous work showed that a single stage rectifier is more efficient in the ultra-low RF power domain than a diode ladder circuit [10]. The experimental results from the previous work showed specifically that at input power levels lower than -25 dBm (the target regime of this work), a single stage harvester provides a greater open circuit voltage than two, three, or four stages. This is because the

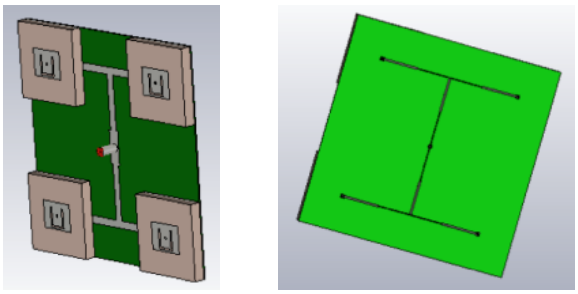

(a) (b)

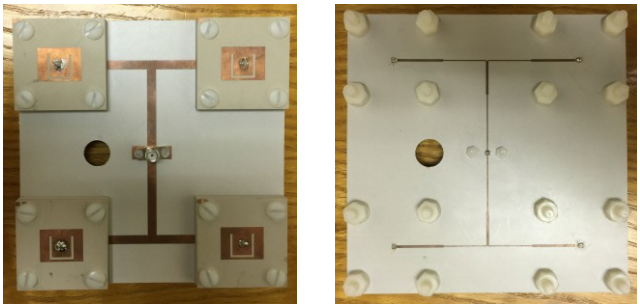

(c) (d)

Fig. 3. (a) front side with elements mounted on H-shaped ground plane, (b) backside parallel feeding network, (c) actual antenna front view, (d) actual antenna rear view.

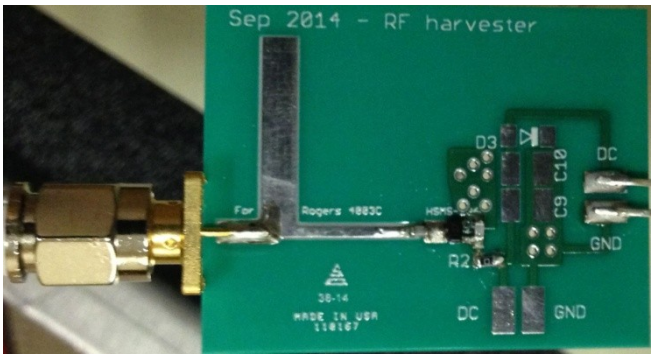

Fig. 4. Rectifier matching circuits.

capacitors and diodes in the circuit are not ideal elements -- diode capacitance can shunt out incremental rectified voltage at higher frequencies (2.4GHz), and the non-ideal IV curves of the diodes show a limited on-current near the diode threshold voltage. A technique for selecting the output capacitor value of the rectifier circuit is described in [14]. A photo of the rectifier circuit and matching network is shown in Fig. 4.

C. DC-DC Boost Converter Design

A typical DC-DC boost converter passes current from an input capacitor through an inductor into an output capacitor under the control of a transistor [15]. High efficiency is possible with a low loss transistor and if the inductor size and switching frequency of the transistor are carefully selected based on the input energy. Previous work uses a MOSFET with a high gate drive voltage from an auxiliary power supply [15]. This cannot start when the auxiliary supply is depleted and is obviously not suitable for an RF energy harvester where the available energy is limited.

The requirement for an auxiliary power supply is addressed in [16] by replacing the MOSFET with an n-channel JFET that can start on voltages as low as 40 to 50 mV. This provides a self-starting and self-oscillating boost converter that is suitable for RF energy harvesting. We improved on this basic design in our previous work by substituting a p-channel JFET that creates a positively biased output voltage [10].

Analysis of our previous booster revealed that choosing different components could significantly improve its performance. Increasing the input capacitance from 100 μF to 660 μF maximizes the stored energy in a reasonable time frame (about 1 min.). If the input capacitance is too high, V_{max} is reduced preventing the booster from reaching battery charge voltage. If the capacitance is too low, the captured energy is reduced thus reducing charging efficiency. The effect of changing the transformer turns ratio on booster performance is shown in Table I where we see that the efficiency, in simulation, is maximized at 1:50. As the turns ratio increases to 1:100, ohmic losses begin to dominate transformer voltage gains.

The oscillation efficiency of the booster is further improved with a different p-channel JFET (changed from the Fairchild MMBF5462 to MMBFJ270). This is illustrated in Fig. 5 that shows the booster input and output voltage for the two JFETs. The MMBFJ270 is more sensitive to lower voltage turn on/off than the MMBF5462 (0.085V vs. 0.17V) and the MMBFJ270 also has a lower V_{gs} threshold of 0.5V as compared to 1.5V for the MMBF5462. The booster is manually switched on when 40 to 50 mV (or more) builds up on the input capacitors. A dedicated circuit will replace this in the future. Fig. 6 shows a schematic.

D. Battery Charger Design

The energy reservoir accumulates ultra-low levels of input power, supplied in bursts, over long periods of time (minutes to hours) so that sensor readings can be taken on a low duty cycle. We considered various capacitor technologies and concluded that none of the commonly available solutions are suitable for our application because their self-discharge rates exceed the energy charging profile we expect to see in practice. This conclusion is based on our study of five alternative storage technologies. We charged three capacitors (100 μF ceramic, polymer, and film) to 1.5V and measured the amount of time it takes them to self-discharge, without a load, to 1.25V. We compared these results to the estimated time it takes a Lithium Polymer (LiPo) rechargeable battery and NiMH rechargeable battery to self-discharge a similar amount. The results in Table II show that the capacitors self-discharge in less than two days. Also, the volume of some options, such as the film capacitor, (greater than 100,000 mm^3), would rule it out for most sensor node applications. The batteries hold their charge for at least a month. We should note that the capacity of the LiPo battery in this test is 50mAh and the NiMH battery is 1.8 mAh. The self-discharge rate of the NiMH battery is estimated from a vendor data sheet under a 1uA drain current with a cutoff voltage of 1.0V (it's not completely self-discharged).

LiPo batteries do not function between 1.5V and 1.25V so we estimated the self-discharge rate of a LiPo battery between 4.1V and 3.85V (a 0.25V drop) from standard rule-of-thumb self-discharge rates of Lithium-ion batteries that are typically 5% in the first 24 hours and 2% per month thereafter.

Rechargeable lithium batteries are commonly used in IOT applications because of their high energy densities [1]. However, they need 4.2V charge pulses and their discharge voltage is between 3.6V and 4.0V. In our application, additional energy-consuming circuitry would be needed to increase the output of the boost converter to this high charging voltage, and again down-regulate to the nominal 1.8V of the loads we anticipate. NiMH batteries, on the other hand, discharge at 1.5V and can be charged at about 2.3 V. In addition, NiMH batteries can be trickle charged indefinitely at voltages lower than 2.3V, but the battery will not reach its full capacity. Because of these characteristics, we chose the NiMH battery and designed a charger that takes advantage of the energy-limited nature of our application. Since we will never charge the battery at a rate greater than its C/10 limit (10% of its charge capacity or 180 µA in our case), over-charge protection circuitry is not required. We use an array of transistors that allows the boost converter to increase the input voltage before gating it into the battery [10].

Table I. Max. efficiency as transformer turns ratio is changed.

transformer turns ratio	maximum efficiency (%)
1:20	6.76
1:50	9.03
1:100	5.29

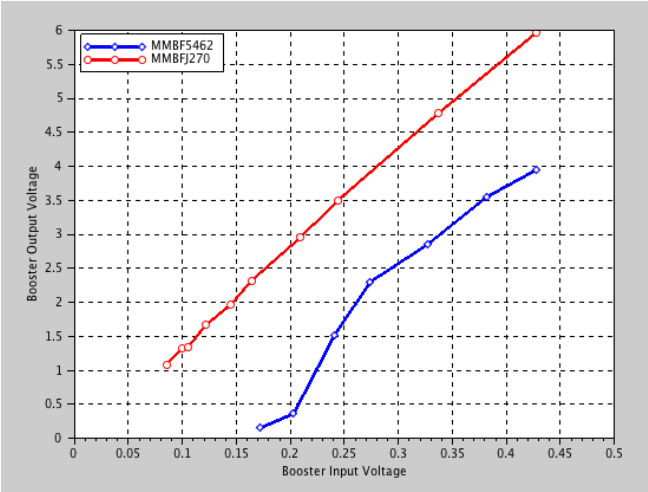

Fig. 5. Boost converter input and output voltage for two p-channel JFETs (MMBF5462 and MMBFJ270).

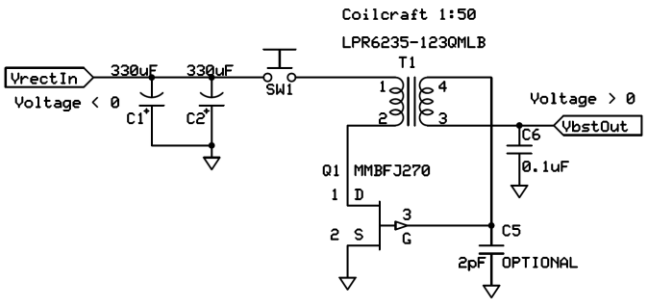

Fig. 6. Boost converter schematic.

Table II. Comparison of capacitor and rechargeable battery technologies.

technology	maximum energy capacity	self-discharge (1.5V to 1.25V)	trickle charge	volume (mm^3)
100 µF ceramic capacitor	112.5 µJ	2.25 hours	1.5 V	3.375
100 µF polymer capacitor	112.5 µJ	39 hours	1.5 V	9.216
100 µF film capacitor	112.5 µJ	7.75 hours	1.5 V	100,625
LiPo rechargeable battery	666 J	30 days	4.2 V	621
NiMH rechargeable battery	9.07 J	50 days	1.5 V	42.3

Previous work [10] used n-channel FETs to switch the ground of the battery terminal as a means of controlling battery charge into the battery. This is not preferred because battery ground is not the same voltage potential as harvesting circuit ground, and therefore any sensing system based on this technology must separate two grounds which adds additional design complexity (and runs the risk of ground loop currents). Furthermore it is not an efficient method of closing a current loop to charge a battery, because parasitic loads which dissipate charged energy are always present. Charge cannot build up as effectively when the battery positive terminal is always connected to the circuit.

Instead, this work uses p-channel FETs and switches the actual charged power into the battery. There is a single ground in the system, and parasitic battery loads have less impact on the charge buildup. Also, this work uses higher switching threshold p-channel MOSFETs that allow the booster to work more effectively by delaying the charger's turn-on time. The p-channel MOSFETs we originally tested included the IRLML6401 (V_{gs}(th) = -0.4V), and the ALD 1117 (V_{gs}(th) = -0.4V). A better choice is the IRF7404 (V_{gs}(th) = -0.7V). The additional 300mV in V_{gs}(th) prevents charge from leaking through the p-channel MOSFET as V_{gs} changes, creating a higher voltage charge pulse, resulting in more power into the battery -- an increase from 10µW to 35µW.

A schematic of the charger circuit is shown in Fig. 7. Specifications for critical parts are given in Table III. A floating gate, precision-trimmed low V_{th} MOSFET is used in the first stage to accurately determine the "kickoff" voltage for the charger circuit, that is, when there has been sufficient energy built up that it should be passed on to the battery for charging (in this case, V_{gs}=1.4V). Two delay stages are used, controlled by MOSFETs U1 and U2, to ensure sufficient build-up of energy from the boost converter before gating it into the battery. The actual power switch gates for U1 and U2 are Q1 and Q2, respectively. The diode D5 prevents any back drive of energy from the battery into the charging circuits when the charger is idle. The impedance of the battery is very low, and the amount of charged energy built up is also very small, so the faster the first rising energy edge into the battery, the more charge the battery receives.

III. RESULTS

A. Measured performance of the antenna

The measured power reflection coefficient (S11) plot of the individual antenna element described above is shown in Fig. 8(a). It has a -10 dB bandwidth of 470MHz centered around the 2.4GHz ISM band. This broad bandwidth is critical to the array design because it enables a broadband antenna array without optimizations of individual elements. The broad bandwidth also provides wide manufacturing tolerances.

The measured gain of each individual antenna element is 4.5dBi. When assembled into the array, the realized gain increases dramatically, to 11.4dBi, with a 10dB bandwidth of 340MHz. However, this antenna array also has strong back lobe gain of 7dBi, which is not ideal for integrating a rectifier on the same PCB board, but can be helpful when the harvesting antenna is mounted in the middle of a room. The measured S11 plot of the array is also shown in Fig. 8(b). The far field realized gain of the antenna array is shown in Fig. 9.

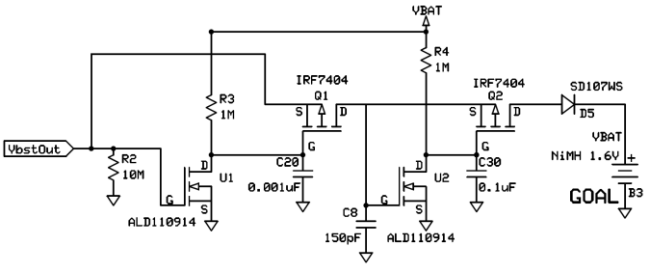

Fig. 7. Battery charger schematic.

Table III. Charger schematic – critical parts list

Part Number	*Reference Designator*	*Threshold Voltage*	*IDSS*
ALD110914SAL	U1, U2	1.4V	400pA
IRF7404TRPBF	Q1, Q2	-0.7V	-1µA

B. Rectifier

The rectifier was connected to the antenna array above and tested at various incident RF power levels (-10dBm to -30dBm) relative to a fixed transmitter. The array antenna was aligned on boresight to the transmitting antenna and tested inside a $1m^3$ anechoic chamber over a distance of 540mm. The transmitting energy source was a continuous wave RF signal at 2450MHz connected to a ground plane monopole antenna. Incident RF power at the harvester was first measured with a spectrum analyzer, and then connected to the rectifier to record open circuit voltage. Fig. 10 shows a comparison of the antenna+rectifier performance of this work compared with other harvesting results in the 2.4GHz frequency band. Note that in particular, this research focuses on the lower, more challenging, RF input energy levels (below -20dBm). Higher rectified output voltages at these lower RF input levels is preferred, to simplify the performance requirements of the boost converter, that boosts the voltage before transferring it into the charger.

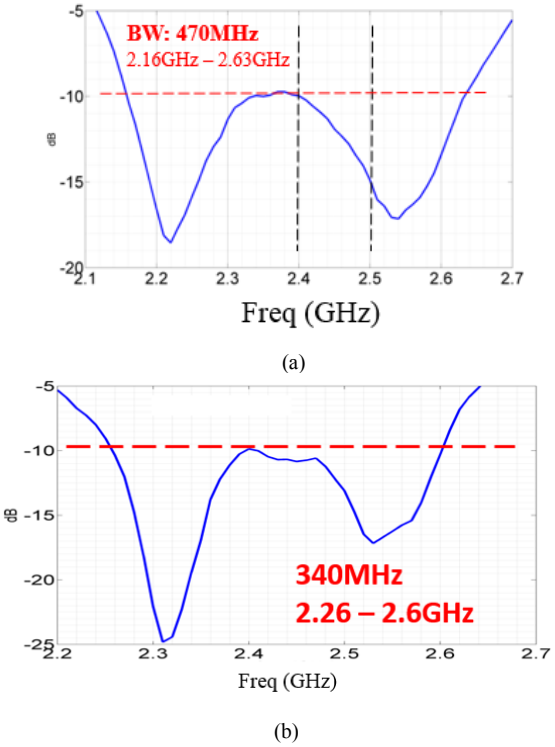

Fig. 8. Measured power reflection coefficient of the individual antenna element (a) and array (b).

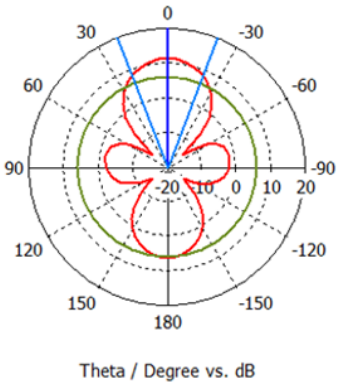

Fig. 9. Far field realized gain for the array antenna.

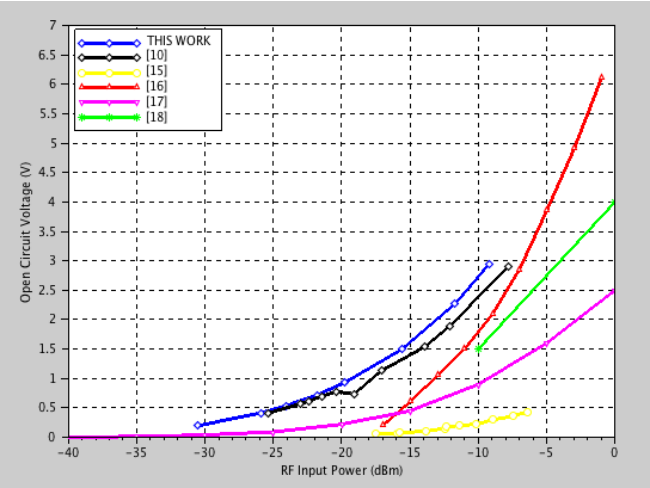

Fig. 10. Antenna + rectifier performance comparison.

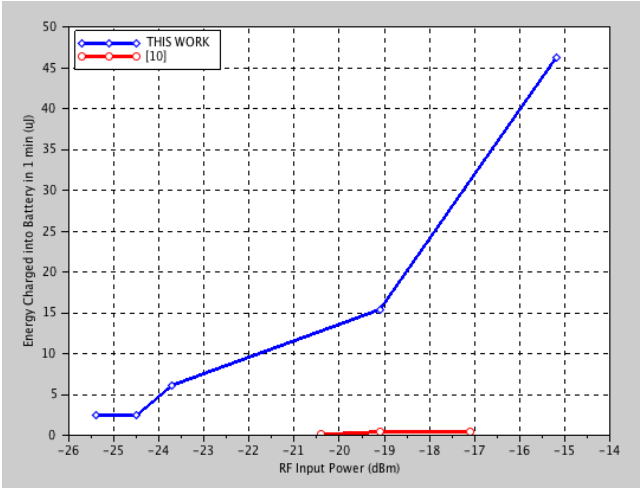

Fig. 12. Energy charged into battery by the charger circuit at different levels of incident RF power, compared to previous work in [10].

C. DC-DC Boost Converter

Fig. 11 compares the performance of the boost converter described in this paper to our previous work [10] and another self-starting and self-oscillating JFET-based design [16]. The input source was a precision DC power supply and the results show that our new design produces output voltages about 1.6X higher than [10] and 2.4X higher than [16]. An RF input source will provide a smaller improvement because it has a higher impedance, but the relative differences between the techniques should be the same.

D. Battery Charger

The results of testing the battery charger (and comparison to previous work) are shown in Figure 12 after approximately one minute of harvesting. The new topology significantly improves on previous results [10] that reported charging the battery with 0.46µJ of energy in one minute at -17.1dBm incident RF input power. The new topology is more efficient because of the high-switching speed p-channel MOSFET transistors (which minimize leakage during the slow-moving transition region), as well as setting the charge-detection points with the very accurate ALD110914 circuit instead of the diode/clamp circuit implemented in [10], which provide an invariable detection point.

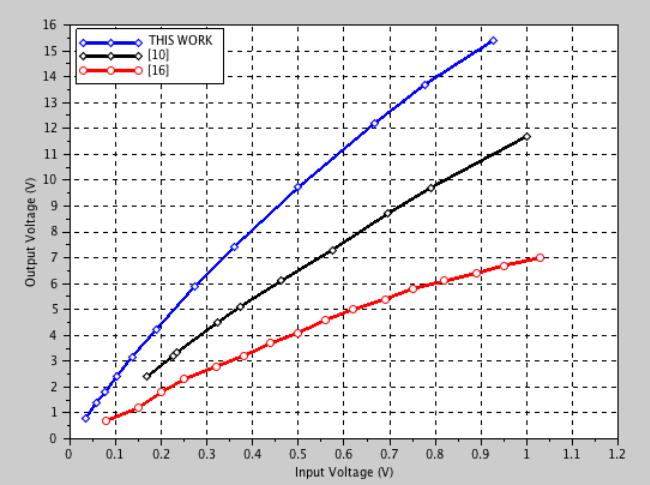

Fig. 11. Boost converter results with DC input.

Charger efficiencies are measured to be greater than 86%, although accurate measurements are challenging because of the dynamic nature of the boost converter under load of the charger.

To measure the charged energy, the voltage drop across a current sense resistor (located between D5 and the battery in Fig. 7) and the actual battery voltage levels were digitized and logged using a National Instruments 9223 high speed ADC. Fig. 13 shows a sample test log from a full end-to-end test of the system environment at -25.4 dBm incident power measured at the feedpoint of the antenna. The top trace is the (inverted) harvested energy from the rectifier into a 660µF capacitive storage bank. The second trace is the boost regulator output voltage (loaded by the charger). The third trace is a measure of voltage into a current sense resistor directly connected to the battery. The final trace is the power driven into the battery as computed by multiplying the voltage by the current through the sense resistor. The charged energy is the integration over time of the power beneath the charge pulse. A SciLab script, run on the ADC log data, was used to compute these values.

IV. FUTURE RESEARCH

Future research includes development of a circuit for automatically transferring charge from the rectifier to the boost converter. Further joint optimization of the components will improve overall efficiency. We will also investigate antenna designs that reduce the alignment sensitivities introduced by the high-gain antenna currently in use.

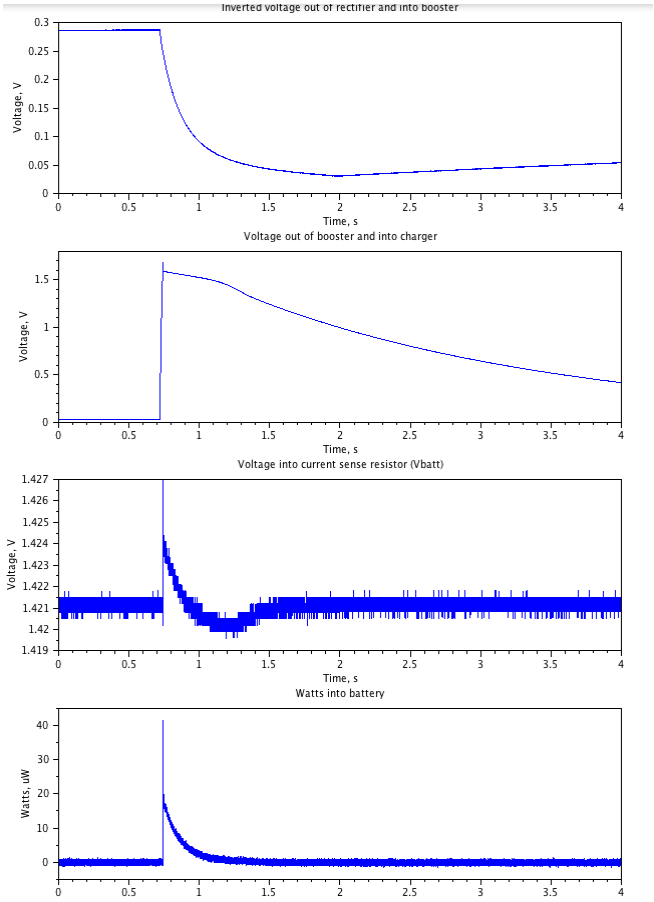

Fig. 13. Logged traces of the battery charger in a full end-to-end test of the system environment at -25.4dBm incident RF power measured at the feedpoint of the antenna. Integrating the power in the charge pulse of the final plot shows 2.08µJ of energy charged into the battery.

V. CONCLUSION

A significantly improved ultra-low power RF energy harvesting system was described that accumulates 2 µJ in a rechargeable NiMH battery in one minute when -25 dBm power is incident at the antenna, as compared to 100 nJ at -20 dBm that was possible with a previous technique [10]. New features include an array antenna with a 11.3 dBi gain. The previous antenna had an 8 dBi gain with the same footprint (120 mm square). Optimization of the boost converter's components increased its output voltage by approximately 60%. Redesign of the battery charger improved the energy harvested in a single pulse by greater than 6X (from 0.33 uJ [10] to 2.08 uJ).

REFERENCES

[1] Y. Lee, S. Bang, I. Lee, Y. Kim, G. Kim, M.H. Gaed, P. Pannuto, P. Dutta, D. Sylvester, and D. Blaauw, "A Modular 1 mm Die-Stacked Sensing Platform With Low Power I C Inter-Die Communication and Multi-Modal Energy Harvesting," IEEE Journal of Solid State Circuits, v. 48, no. 1, Jan. 2013, pp. 229-243.

[2] M. Feldmeier and J.A. Paradiso, "Personalized HVAC System," Internet of Things (IOT), IEEE, Tokyo, Dec. 2010. [Online] Available: http://dblp.uni-trier.de/db/conf/iot/iot2010.html#FeldmeierP10

[3] G. Kim, Y. Lee, Z. Foo, P. Pannuto, Y. Kuo, B. Kempke, M.H. Ghaed, S. Bang, I. Lee, Y. Kim, S. Jeong, P. Dutta, D. Sylvester and D. Blaauw, "A millimeter-scale wireless imaging system with continuous motion detection and energy harvesting," 2014 IEEE Symposium on VLSI Circuits, June 10, 2014, pp. 1-2.

[4] J. Bryzek, "Roadmap for the Trillion Sensor Universe, " Berkeley, CA, April 2, 2013. [Online] Available: http://www-bsac.eecs.berkeley.edu/scripts/show_pdf_publication.php?pdfID=1365520205

[5] K. Gudan, S. Chemishkian, J.J. Hull, M. Reynolds, S. Thomas, "Feasibility of wireless sensors using ambient 2.4GHz RF energy," in Sensors, 2012 IEEE. doi: 10.1109/ICSENS.2012.6411176

[6] H. Visser, A. Reniers, and J. Theeuwes, "Ambient RF energy scavenging: GSM and WLAN power density measurements," in Proc. 38th European Microwave Conf., Amsterdam, 2008, pp. 721-724.

[7] D. Bouchouicha, M. Latrach, F. Dupont, and L. Ventura, "An experimental evaluation of surrounding RF energy harvesting devices," in Proc. 40th European Microwave Conf., Paris, 2010, pp. 1381-1384.

[8] S. Kitazawa, H. Ban, and K. Kobayashi, "Energy harvesting from ambient RF sources," in Microwave Workshop Series on Innovative Wireless Power Transmission: Technologies, Systems, and Applications (IMWS), 2012 IEEE MTT-S International, Kyoto, pp. 39-42.

[9] H. Nishimoto, Y. Kawahara, and T. Asami, "Prototype implementation of ambient RF energy harvesting wireless sensor networks," in Sensors, 2010 IEEE, Kona, HI, 2010, pp. 1282-1287.

[10] K Gudan, S. Chemishkian, J.J. Hull, S.J. Thomas, J. Ensworth, and M.S. Reynolds, "A 2.4GHz Ambient RF Energy Harvesting System with -20dBm Minimum Input Power and NiMH Battery Storage," in RFID Technology and Applications Conference (RFID-TA), Tampere, Finland, 2014.

[11] C. Valenta and G. Durgin, "Harvesting Wireless Power: Survey of Energy-Harvester Conversion Efficiency in Far-Field Wireless Power Transfer Systems," IEEE Microwave Magazine, v. 15, no. 4, June, 2014, 108-120.

[12] S. F. Maharimi. M.F.A. Malek, M.F. Jamlos, S.C. Neoh, and M. Jusoh, "Impact of Spacing and Number of Elements on Array Factor," in PIERS Proceedings, Kuala Lumpur, Malaysia, 2012.

[13] M. Huque, M.K. Hosain, M.S. Islam, and M.A. Chowdhury, "Design and Performance Analysis of Microstrip Array Antennas with Optimium Parameters for X-band Applications," in International Journal of Advanced Computer Science and Applications, Vol. 2, No. 4, 2011.

[14] J. Ensworth, S. Thomas, S. Shin, and M. Reynolds, "Waveform-aware ambient RF energy harvesting", in Proc. IEEE Int. Conf. on RFID, Orlando, FL, 2014, pp. 67-73.

[15] H.Hong, X. Cai, X. Shi, and X. Zhu, "Demonstration of a highly efficient RF energy harvester for Wi-Fi signals," in Proc. Int. Conf. on Microwave and Millimeter Wave Technology (ICMMT), vol. 5, Shenzhen, 2012. doi: 10.1109/ICMMT.2012.6230448

[16] S. Adami, V. Marian, N. Degrenne, C. Vollaire, B. Allard, and F. Costa, "Self-powered ultra-low power DC-DC converter for RF energy harvesting," in Proc. Faible Tension Faible Consommation (FTFC), 2012 IEEE. doi: 10.1109/FTFC.2012.6231746

[17] U. Olgun, C. Chen, and J. Volakis, "Design of an efficient ambient WiFi energy harvesting system," in IET Microwaves, Antennas & Propagation, vol. 6, no.11, pp. 1200-1206, 2012.

[18] K. Agarwal, T. Mishra, M.F. Karim, Nasimuddin, M.O.L. Chuen, Y.X. Guo, and S.K. Panda, "Highly efficient wireless energy harvesting system using metamaterial based compact CP antenna," in Microwave Symposium Digest (IMS), 2013 IEEE MTT-S Int, Seattle, WA. doi: 10.1109/MWSYM.2013.6697693